

THREE-DIMENSIONAL AMR SIMULATIONS OF LONG-DURATION GAMMA-RAY BURST JETS INSIDE MASSIVE PROGENITOR STARS

D. LÓPEZ-CÁMARA^{1, *}, BRIAN J. MORSONY², MITCHELL C. BEGELMAN^{3, 4}, DAVIDE LAZZATI¹

Draft version November 5, 2018

ABSTRACT

We present the results of special relativistic, adaptive mesh refinement, 3D simulations of gamma-ray burst jets expanding inside a realistic stellar progenitor. Our simulations confirm that relativistic jets can propagate and break out of the progenitor star while remaining relativistic. This result is independent of the resolution, even though the amount of turbulence and variability observed in the simulations is greater at higher resolutions. We find that the propagation of the jet head inside the progenitor star is slightly faster in 3D simulations compared to 2D ones at the same resolution. This behavior seems to be due to the fact that the jet head in 3D simulations can wobble around the jet axis, finding the spot of least resistance to proceed. Most of the average jet properties, such as density, pressure, and Lorentz factor, are only marginally affected by the dimensionality of the simulations and therefore results from 2D simulations can be considered reliable.

Subject headings: gamma-ray bursts: general — hydrodynamics — supernovae: general

1. INTRODUCTION

Long-duration gamma-ray bursts (GRBs) are produced by collimated relativistic outflows (Sari et al. 1999) ejected in the core of massive stars at the end of their evolution (Woosley 1993; Hjorth et al. 2003; Stanek et al. 2003; Woosley & Bloom 2006). Since their relativistic outflows have to propagate through their progenitor star material and exit the star before producing the gamma-ray photons, an outstanding issue with this scenario is to understand the mechanisms that prevent the entrainment of baryons in the light, hot jet (MacFadyen & Woosley 1999; Aloy et al. 2000).

On the other hand, even if the jet-star interaction cannot slow down the jet, it has a strong impact on its dynamics (Morsony et al. 2007) and can supply enough energy to explode the star as a supernova (Khokhlov et al. 1999; MacFadyen et al. 2001; Wheeler et al. 2002; Maeda & Nomoto 2003; Lazzati et al. 2012). In most cases, the study of the jet-star interaction has been performed numerically, with analytic models used only for guidance (Aloy et al. 2002; Gómez & Hardee 2004; Morsony et al. 2007; Matzner 2003; Bromberg et al. 2011). Even so, studying the propagation of a relativistic outflow that is continuously shocked by a much denser environment is not trivial since the length-scale of features in the relativistic material is typically $\sim R/\Gamma$ and therefore a large dynamical range is involved. When possible, adaptive mesh refinement (AMR) codes have been adopted (Morsony et al. 2007, 2010; Lazzati et al. 2009, 2010, 2011b; Nagakura et al. 2011), and the simulations have been limited to two dimensions (MacFadyen & Woosley 1999;

Aloy et al. 2000; MacFadyen et al. 2001; Zhang et al. 2003; Mizuta et al. 2006; Morsony et al. 2007, 2010; Lazzati et al. 2009, 2010, 2011b; Mizuta & Aloy 2009; Nagakura et al. 2011). These studies have shown that even though the jet material is relativistic, the jet-head propagates sub-relativistically inside the star, thereby allowing causal contact between the bow shock at the head of the jet and the star. The shocked star material therefore drains at the sides of the jet producing a hot cocoon (Ramirez-Ruiz et al. 2002; Lazzati & Begelman 2005) instead of being entrained in the jet.

Two dimensional (2D) simulations can provide important answers to the outstanding questions listed above. However, they are plagued by artifacts due to the presence of a symmetry axis in the center of the jet. First, a plug of dense material accumulates in front of the jet head, slowing down its propagation and creating plumes of hot plasma at wide angles (see Figure 1 in Lazzati et al. (2010) for an example). Second, recollimation shocks coming from the sides of the jet bounce strongly off the jet axis in 2D simulations, while they could dissipate more efficiently in a simulation at the natural dimensionality. Finally, the role of turbulence and instabilities cannot be properly explored in 2D simulations. Wang et al. (2008) found that in some cases a three dimensional (3D) relativistic jet would break apart and not be able to produce a successful GRB (while in 2D it would produce a successful GRB).

While 3D simulations of GRB jets have been attempted in the past (Zhang et al. 2004), they were performed with a fixed grid code, casting doubt on their capability to resolve the required small scales. A 3D test-case with AMR was presented by Wang et al. (2008), but since the jet-progenitor evolution varied drastically as a function of the numerical resolution (unlike our study), not much could be inferred from their study. Thus, in this paper we present, for the first time, 3D adaptive mesh refinement (AMR) simulations of GRB jets crossing a pre-SN progenitor and then flowing through the interstellar medium.

This paper is organized as follows. We first describe

¹ Department of Physics, NC State University, 2401 Stinson Drive, Raleigh, NC 27695-8202, USA

² Department of Astronomy, University of Wisconsin-Madison, 2535 Sterling Hall, 475 N. Charter Street, Madison WI 53706-1582, USA

³ JILA, University of Colorado, 440 UCB, Boulder, CO 80309-0440, USA

⁴ University of Colorado, Department of Astrophysical and Planetary Sciences, 389 UCB, Boulder, CO 80309-0389, USA

* dlopezc@ncsu.edu

the physics, initial setup, and the numerical simulations in Section 2, followed by our results and discussion in Section 3. Conclusions are given in Section 4.

2. PHYSICS, INITIAL SETUP AND SIMULATIONS

2.1. Physics and initial setup

As what now seems to be the generic model used for long GRBs (Morsony et al. 2007, 2010; Lazzati et al. 2009, 2011a,b, 2012; López-Cámara et al. 2009, 2010; Lindner et al. 2010, 2012; Nagakura et al. 2011, for example), we consider the one-dimensional (1D) pre-supernova 16TI model from Woosley & Heger (2006) as our initial stellar configuration. Initially (in the zero-age main sequence) model 16TI is a $16 M_{\odot}$ Wolf-Rayet star with $0.01 Z_{\odot}$ metallicity, and 3.3×10^{52} erg s equatorial angular momentum. The final outcome of such model is a pre-SN progenitor with $13.95 M_{\odot}$ and nearly half the size of the sun ($R_0 = 4.1 \times 10^{10}$ cm). Assuming spherical symmetry, the 1D density and pressure profiles were mapped onto a 3D configuration that we assumed to be initially without rotation. The internal energy and the temperature were calculated assuming a relativistic polytropic equation of state ($\gamma=4/3$). The pre-SN progenitor was immersed in an interstellar medium (ISM) with constant density ($\rho_{\text{ism}} = 10^{-10}$ g cm $^{-3}$). Even though a wind environment would probably be more appropriate, we note that within the size of our simulation the dynamical role of the ambient medium is negligible and the results are therefore insensitive to the chosen ambient medium profile.

A relativistic jet commencing its flow at the center of the pre-SN progenitor was imposed at all times as a boundary inflow condition. The jet was launched at the center of the star (in fact slightly above it), flowing upwards in the polar direction ($x=z=0$, $y=R_i=10^9$ cm). The imposed jet had a half-opening angle of $\theta_0=10^\circ$, a constant luminosity of $L_0 = 5.33 \times 10^{50}$ erg s $^{-1}$, an initial Lorentz Factor of $\Gamma_0=5$, and a ratio of internal over rest-mass energy equal to $\eta_0=80$ (Morsony et al. 2007, 2010; Lazzati et al. 2009). In order to break the 2D axis symmetry, the jet was slightly asymmetric. For the latter, we set the jet with a 1% density and pressure asymmetry on either side of a line in the XZ plane 40 degrees from the X axis. Differently from Wang et al. (2008) (3D numerical study in which a two dimensional symmetrical initial setup was assumed) our initial setup resembles that from model 3A in Zhang et al. (2004) enhanced with a small perturbation in the jet.

2.2. Numerical simulations

In order to follow the temporal evolution of our initial setup, we solved the 3D gas-dynamic equations using the FLASH code (version 2.5) in cartesian coordinates (Fryxell et al. 2000). The simulation domain covered the top half of the pre-SN progenitor star as well as the ISM it is immersed in (see for example panel *a* from Figure 1). The boundaries were set at $y_{\text{min}}=10^9$ cm, $y_{\text{max}}=2.4 \times 10^{11}$ cm, $x_{\text{max}}=-x_{\text{min}}=6 \times 10^{10}$ cm, and $z_{\text{max}}=-z_{\text{min}}=6 \times 10^{10}$ cm. Only the equatorial plane ($y=y_{\text{min}}$) was set with a reflective boundary condition, all the other boundaries were set with transmission conditions. We used a 10-level binary adaptive grid with square-shaped pixels ($\Delta x =$

$\Delta y = \Delta z \equiv \Delta$). The highest refinement level (also referred to as the finest resolution level) were accessible only at the core of the pre-SN star where the jet is injected and initially propagates. Moving away from the stellar core, the maximum level of refinement was progressively decreased. In practice, the base of the jet had the finest resolution at all times and the three next finest levels followed the jet (and the polar part of the cocoon) as it drilled through the progenitor.

Two set of simulations with a different value of Δ were performed. We will refer to the the high resolution model as ‘‘HR’’, and the low resolution as ‘‘LR’’. The HR model had the finest resolution (covering the core of the star at all times) equal to $\Delta = 3.125 \times 10^7$ cm, the jet for this case was followed with a resolution of at least $\Delta = 1.25 \times 10^8$ cm. The LR model had the same setup but the value of the the finest resolution was set equal to $\Delta = 6.25 \times 10^7$ cm, and the jet was followed with a resolution of at least $\Delta = 2.5 \times 10^8$ cm. The resolution with which we follow the jet is comparable to that from the 3D collapsar study of Zhang et al. (2004) (where the maximum resolution was $\Delta \sim 10^8$ cm), and to the most recent 3D GRB jet study from Wang et al. (2008) (where $\Delta = 7 \times 10^7$ cm). The resolution with which we resolve the core of the star is comparable to that from previous 2D GRB jet numerical studies (Zhang et al. 2003; Mizuta et al. 2006; Morsony et al. 2007; Nagakura et al. 2011). In order to understand the three-dimensional effects properly, we also ran an extra two dimensional model.

Differently from the 3D simulation, the 2D run was performed in cylindrical coordinates, the polar axis being coincident with the jet axis. The 2D model had an initial configuration akin to the XY and the ZY planes of the 3D model. The 2D model had the same input physics and resolution as that of the 3D HR model. A summary with the differences between the numerical models is shown in Table 1.

TABLE 1
MODEL CHARACTERISTICS

Model	Δ in core ($\times 10^7$ cm)	Δ in jet ($\times 10^8$ cm)
3D LR	6.250	2.50
3D HR	3.125	1.25
2D HR	3.125	1.25

3. RESULTS AND DISCUSSION

3.1. Global morphology.

In Figure 1 we show the density stratification maps for the XZ, XY, and ZY planes for the 3D LR model. Each panel shows a different timeframe: a. $t_a = 2.7$ s; b. $t_b = 4.2$ s; c. $t_c = 5.3$ s; d. $t_d = 7.3$ s; and e. $t_e = 9.3$ s. These panels are arranged to illustrate the jet-progenitor-ISM temporal evolution (animations of the density stratification map, Lorentz factor, radial density, radial Lorentz factor, and Schlieren map in the XY plane, are linked to the online version of this manuscript). The morphology of our system is divided into two main

phases: when the jet moving inside the progenitor and when the jet has broken out of the star and interacts with the interstellar medium. Such temporal evolution is consistent with what has already been seen in previous numerical studies (Zhang et al. 2003; Morsony et al. 2007). Superimposed on the density stratification in Figure 1, we show the isocontour levels corresponding to 10^{-4} , 10^{-2} , 1, 10^2 , and 10^4 (all in g cm^{-3}), these isocontour levels are shown in Figure 2.

The $t_{\text{bo}}=4.2$ s breakout time is similar to (but somewhat shorter than) that already seen in previous collapsar studies (Zhang et al. 2003, 2004; Morsony et al. 2007, 2010). Depending on the progenitor that one chooses, and the particular characteristics of the jet, it takes 5 to 10 s to cross the stellar envelope. Compared to power-law stellar models, the models from Woosley & Heger (2006) are more compact and dense and it takes less time for the jet to cross the realistic progenitors (Mizuta et al. 2006). Our t_{bo} is very similar to the breakout time computed with the analytical model from Bromberg et al. (2011). Still, it must be stated that since the jet in our numerical simulations is launched at an inner radius which is at least 10^4 times the gravitational radius ($R_i \sim 10^4 R_g$ for a $1.4M_{\odot}$ black hole), the jet from the simulations is somewhat wider than that from the analytical model and thus it propagates slower. The t_{bo} for our study implies that the average propagation velocity of the jet inside the star is $\sim 0.32c$. The jet, composed of low density material, has its initial opening angle reduced by relativistic hydrodynamic collimation effects.

Once the jet crosses the stellar envelope and breaks out of the surface, the cocoon (which surrounds the jet and is present since its formation) expands through the ISM (Ramirez-Ruiz et al. 2002; Lazzati & Begelman 2005), differently from when the jet is drilling through the progenitor when the cocoon is bound inside the star and close to the jet. When the jet breaks out of progenitor it becomes uncollimated and the cocoon moves out in the polar direction (moving parallel to the jet), also expanding sideways on top of the stellar surface. Such spreading (see panel c, d, and e from Figures 1-2) was predicted by the analytic solution from Bromberg et al. (2011). By this time not only does the cocoon present zones where variability is clearly present, but also the jet presents turbulent-like structures. The variability in the cocoon is due to the fact that the jet-cocoon system is at least five orders of magnitude denser than the surrounding ISM. Hence, any instability that forms on the cocoon's boundary or that travels upwind from the jet into the cocoon is not dissipated. Due to the location of the outer boundaries, we are not able to follow the jet-cocoon-ISM system entirely after approximately 10 s. By this time the cocoon has crossed the outer boundaries (the jet crosses the top boundary at approximately 13 s). Also, it must be noted that as time passes the inner isocontour ($\rho=10^4 \text{ cm g}^{-3}$) disappears. This is due to the reverse shock, which is expanding and pushing the dense material outwards. Such behavior has already been seen in the study of Lazzati et al. (2010).

3.2. Symmetry loss

To understand when the cylindrical symmetry is broken, in Figure 3 we plot the radial density distribution as well as the energy density (U , in erg cm^{-3}) for four dif-

ferent paths which move along a cone of 2° half-opening angle (with its origin set at $x=y=z=0$) for model 3D LR. One of these paths moves radially (R) along the “(+X,+Z)” quadrant; another moves in the “(+X,-Z)” quadrant; another in the “(-X,+Z)” quadrant, and finally a path which moves along the “(-X,-Z)” quadrant.

Consistently with previous 2D and 3D collapsar simulations (Zhang et al. 2003, 2004; Mizuta et al. 2006; Nagakura et al. 2011), we see that as the jet drills through the stellar envelope a complex shock system forms, characterized by a forward and a reverse shock at the head of the jet and by a series of conical recollimation shocks. The first recollimation shock, visible almost at the base of the jet, seems to be static (at $R\sim 2\times 10^9 \text{ cm}$), but this is due to the fact that it moves at relativistic speed in the rest-frame. Since the study of the shock structure is not our goal, we do not focus on the nature of these shocks, nor do we need to know where the contact discontinuity is set. For the sake of our study all we need to be able to discern is the stellar and jet material that has and has not been shocked.

Specifically, the regions which we will be addressing to in the rest of the discussion will be the shocked (SJ) and unshocked (UJ) parts of the jet. The UJ material maintains its initial density profile, while the SJ material breaks the symmetry in the 3D numerical simulations. The density profile can vary up to two orders of magnitude for different locations at the same distance from the progenitor center; on the other hand, the UJ varies less than an order of magnitude. As the jet crosses through the progenitor star its density decreases as a function of time (see Figure 4). Before the jet breaks out from the stellar surface, the density profile inside the progenitor follows a quasi-constant profile which for t_{bo} is $\sim 10^{-1} \text{ g cm}^{-3}$. Then, when the jet breaks out of the stellar surface, it recovers a decaying radial density profile that for 9.3 s reaches density values as low as $10^{-5} \text{ g cm}^{-3}$.

3.3. Lorentz factor evolution

In Figure 5 and Figure 6 we show the temporal evolution for the Lorentz factor (with the velocity field also present); and the radial Lorentz factor profile along the 2° radial path for model 3D LR. Before the breakout time only a relativistic jet (with $\Gamma \sim 10$) is present (see panel with $t=4.2$ s from Figure 5). In Figure 6 we see that the SJ material for $t < t_{\text{bo}}$ (blue, red and green lines) reaches values close to $\Gamma = 15$; and the UJ Lorentz factor remains practically the same as the initial Lorentz factor ($\Gamma_0=5$). This behavior is consistent with what has already been seen in previous GRB jet numerical simulations where the initial Lorentz factor, prior to t_{bo} , reaches values close to 10 (Zhang et al. 2004; Mizuta et al. 2006). Once the jet breaks out of the stellar surface, the jet is accelerated. The high internal energy is able to accelerate material with Lorentz factors values of order $\Gamma \sim 100$ in some zones. If accelerated with no energy dissipation, the jet's maximum Lorentz factor would be 400 ($\Gamma_{\infty}=\Gamma_0\eta_0$) (Morsony et al. 2007). In the panel with $t=5.3$ s from Figure 5 (brown line in Figure 6) we show how the jet's forward shock and the recently formed cocoon produce a “mushroom-like” high- Γ structure. At later times ($t > t_{\text{bo}}$) (orange, cyan and black lines in Figure 6) the mushroom-like structure grows bigger and its

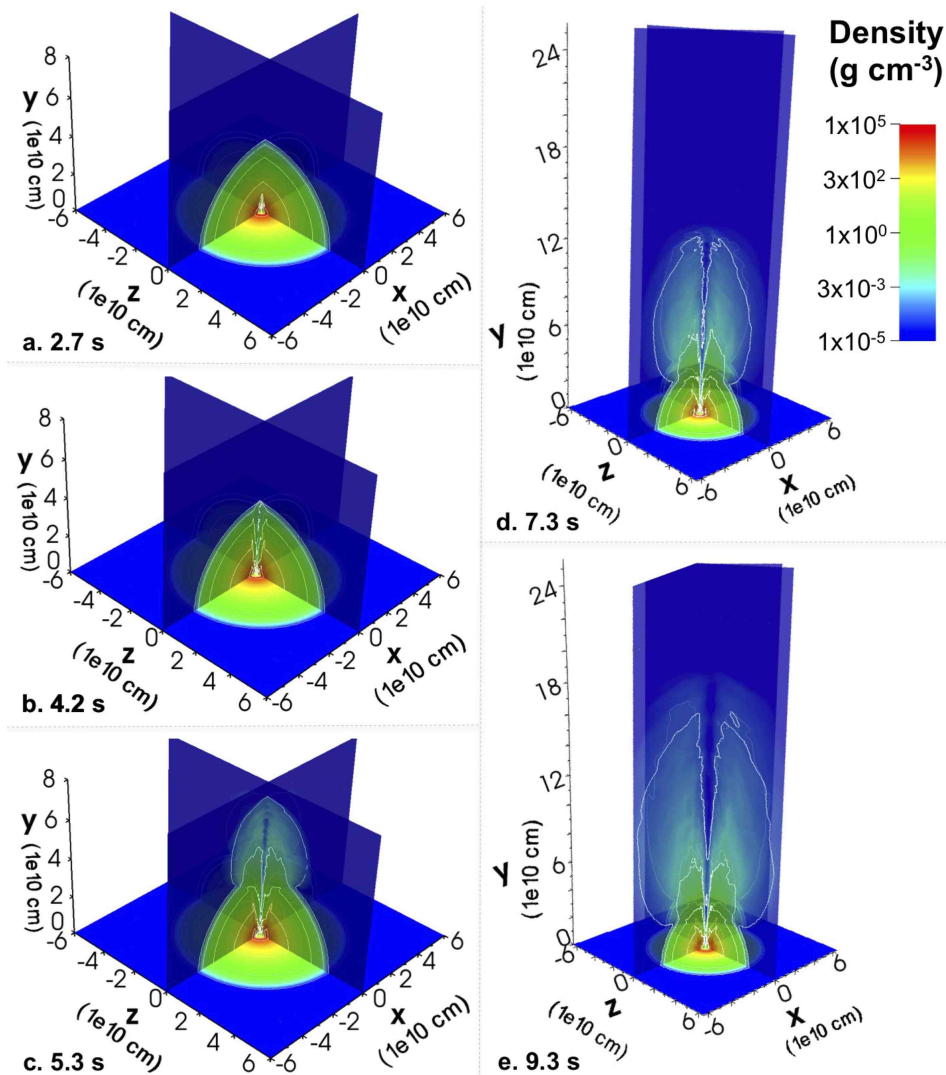


FIG. 1.— Density stratification maps (g cm^{-3}) for different timeframes (a. 2.7 s; b. 4.2 s; c. 5.3 s; d. 7.3 s; e. 9.3 s) for model 3D LR. The isocontour levels correspond to: 10^4 g cm^{-3} ; 10^2 g cm^{-3} ; 1 g cm^{-3} ; $10^{-2} \text{ g cm}^{-3}$; $10^{-4} \text{ g cm}^{-3}$. In order to better visualize the internal structure in the pre-SN, the minimum value in all the density stratification plots was set to $10^{-5} \text{ g cm}^{-3}$. A movie of this figure is available in [http://www4.ncsu.edu/~dlopez/Simulations_\(published\).html](http://www4.ncsu.edu/~dlopez/Simulations_(published).html)

Lorentz factor Γ increases significantly.

To see the high Lorentz factor material in the jet, in Figure 7 we plot the Γ isocontours for $t=9.3 \text{ s}$. By this time the mushroom structure is evident and also certain regions in the polar axis reach Lorentz factor values as high as $\Gamma = 50$ (pink isocontours). Unfortunately our numerical domain does not permit us to follow such high- Γ regions and they escape the top boundary after approximately 10 seconds. This is once more congruent with the results from previous studies where after the t_{bo} the cocoon reaches values as high as $\Gamma \sim 15$, and the jet values of order $\Gamma \sim 100$ (Mizuta et al. 2006). It must also be noted that when the jet breaks out of the stellar surface, a low-speed wind forms. This wind expands isotropically from the point in the stellar surface where the jet drilled through, and moves at an average speed vastly inferior ($v \leq 0.01 c$) to that of the jet.

3.4. Resolution effects

In order to be able to evolve the initial setup up to integration times of order $\sim 10 \text{ s}$ and to resolve the jet-progenitor with a suitably fine grid an AMR mesh was used. In Figure 8 we show the fraction of the volume that the three finest resolution levels occupied as a function of time. The finest grid level, the one with which the base of the jet was resolved ($\Delta \sim 10^7 \text{ cm}$, red line in Figure 8) occupied less than 10^{-7} of the entire volume. Meanwhile, the two next finest levels, which followed the propagation of the jet through the progenitor ($\Delta \sim 10^8 \text{ cm}$, blue and green lines in Figure 8), occupied less than 10^{-6} and 10^{-4} of the volume. Needless to say, if we had used a fixed mesh with a comparable resolution to that with which the base of the jet was resolved, it would have required $\sim 10^6$ more computational power (compared the computational power used in our simulations), and thus the benefit from using an AMR scheme.

To verify that the evolution of the jet from our results is not dependent on the numerical resolution, we ran a

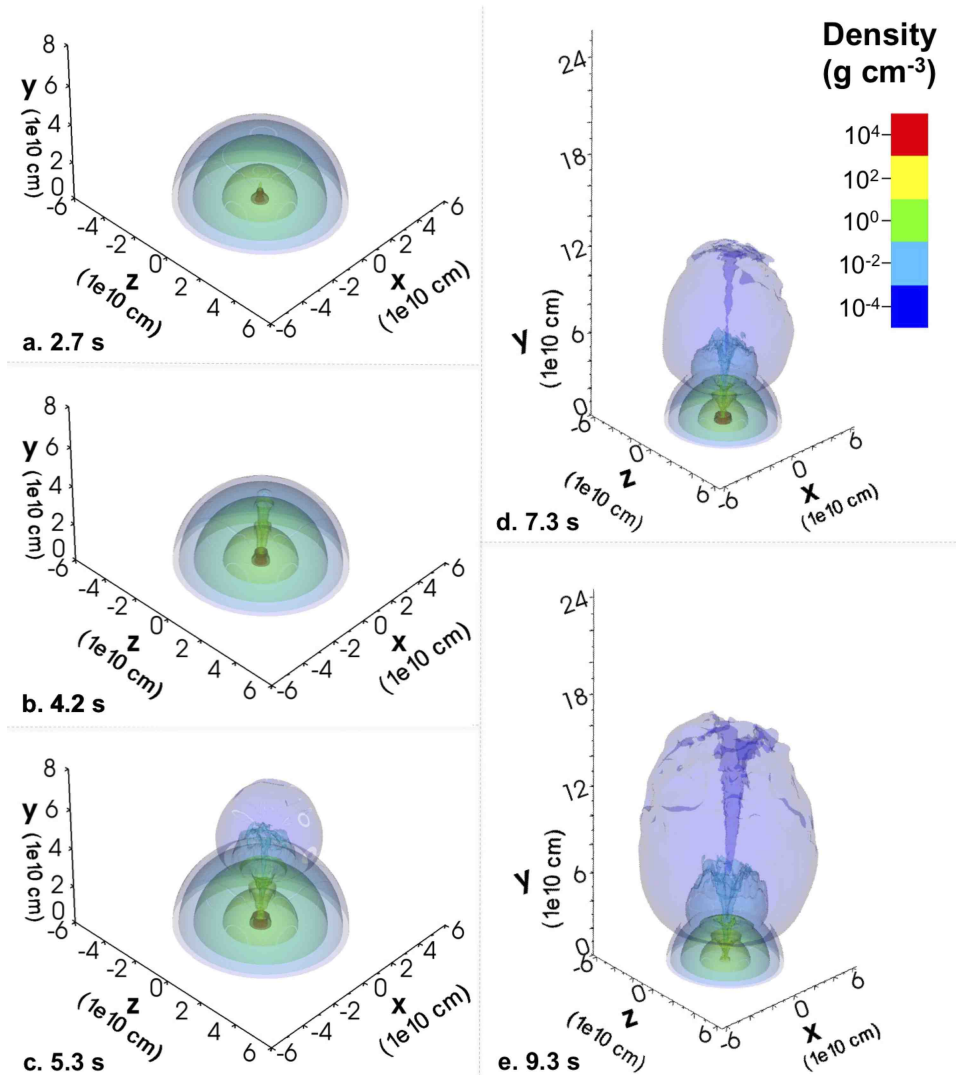


FIG. 2.— Density stratification map for different isocontour levels (red= 10^4 g cm^{-3} ; yellow= 10^2 g cm^{-3} ; green= 1 g cm^{-3} ; cyan= $10^{-2} \text{ g cm}^{-3}$; blue= $10^{-4} \text{ g cm}^{-3}$) for model 3D LR. The timeframes are the same as those indicated in Figure 1. A movie of this figure is available in [http://www4.ncsu.edu/~dlopez/Simulations_\(published\).html](http://www4.ncsu.edu/~dlopez/Simulations_(published).html)

new model with the same setup and physics but with a maximum resolution two times finer than for the low resolution (see Section 2.2 for details). In Figure 9 we show the density profiles for the 3D HR and 3D LR case. In each case we show the two main phases already discussed in Section 3.1: prior to the breakout phase; the breakout; and the post breakout phase. We must note that the selected timeframes for each of the phases were chosen arbitrarily so that the LR and HR cases resemble each other, and hence their basic morphology characteristics can be compared. The main result is that the basic morphology characteristics from each phase (see discussion in Sections 3.1–3.3), are well reproduced independently of the numerical resolution. Unlike the results from the numerical 3D jet GRB study from Wang et al. (2008) where high resolution models gave qualitatively different jet dynamics, we obtain consistent jet behavior independently of the resolution.

Among the differences associated with the resolution, are a higher level of turbulence and a slower advance of

the jet head in the HR model. The latter’s jet moves $\sim 20\%$ slower than the LR case, hence the breakout time for the HR case is $t_{\text{bo}}=5.1 \text{ s}$. The jets velocity resolution difference is due to the fact that the HR case has a wider jet ($\sim 5\%$ wider than the LR case). Since we are powering both jets equally, the narrow-LR jet will move faster. The turbulence resolution difference is due to the fact that the LR simulation has higher diffusion, and thus suppresses the small scale instabilities which are present in the HR model. The higher amount of turbulence in the HR model also slows it down (compared to the LR model), this due to the fact that a larger fraction of the energy is converted into turbulence. Hence, reducing the HR jet’s kinetic energy and ram-pressure. We must note that these two resolution effects are consistent with what has already been seen in previous jet-collapsar simulations, for example Morsony et al. (2007). Even though the latter study is a two-dimensional one, it also presents more vortices in the HR than in the LR case.

To illustrate how in the HR model there is more vari-

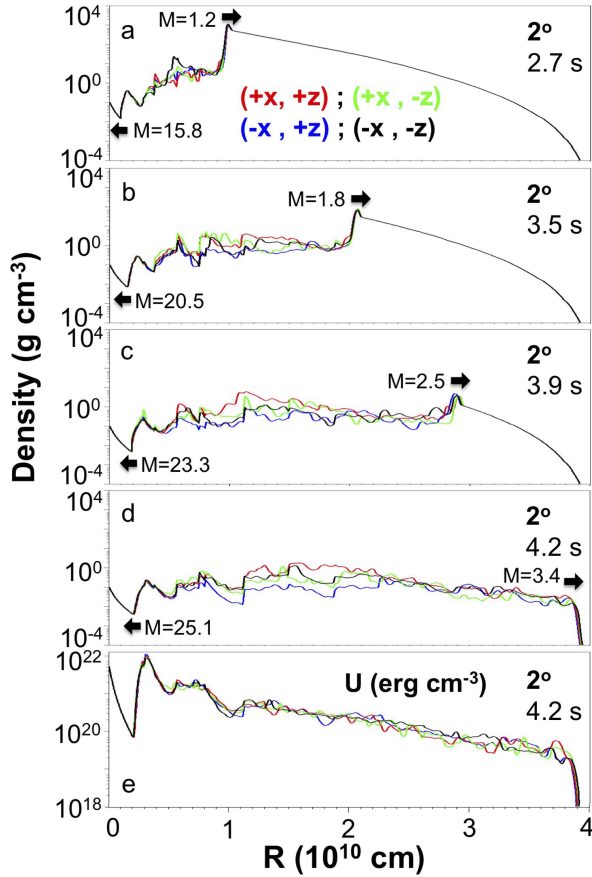


FIG. 3.— Radial profiles for different 2° paths and times for model 3D LR. Panel a through d show different radial density profiles (g cm^{-3}), panel e shows different energy density profiles (erg cm^{-3}). Each of the radial paths commences in the origin and runs through different quadrants: (+X,+Z) quadrant (red line); (+X,-Z) quadrant (green line); (-X,+Z) quadrant (blue line); (-X,-Z) quadrant (black line). Each panel corresponds to a different timeframe: a. 2.7 s, b. 3.5 s, c. 3.9 s, d. and e. 4.2 s. The forward and reverse shock Mach number for each timeframe are also indicated. A movie of this figure is available in [http://www4.ncsu.edu/~dlopez/Simulations_\(published\).html](http://www4.ncsu.edu/~dlopez/Simulations_(published).html)

ability than in the LR one, in Figure 10 we plot the radial density profiles for both resolution models. The upper panel of Figure 10 is the radial density profile for a path within the jet (specifically a 2° path), while the lower panel is the radial density profile in the edge of the jet (10° path). Inside the jet, there is no major difference between the two resolution models. On the other hand, at the edge of the jet the numerical resolution clearly affects the density profile. Here the HR presents numerous depressions in the density radial profile while the LR case has a radial profile which follows a smoother distribution with less depressions and variability.

We also analyzed the effects of numerical resolution on the jet's Lorentz factor distribution. Before the jet breaks out, apart from the velocity with which the jet evolves, there is no clear difference between the low and high resolution models. But at $t > t_{\text{bo}}$ there are morphological changes due to the resolution. Figure 11 shows the Lorentz factor map for the 3D LR and the 3D HR models just after breaking out of the stellar surface. The Lorentz factors are comparable but, as expected, the HR

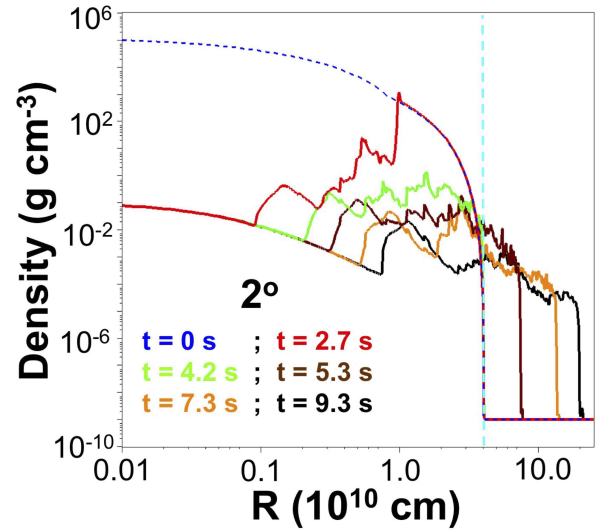


FIG. 4.— Time evolution (0 s; 5.3 s; 7.3 s; 9.3 s) for the 2° radial density profile (g cm^{-3}) from the (+X,+Z) quadrant (black line in Figure 3). The stellar surface is indicated by the cyan dashed line. A movie of this figure is available in [http://www4.ncsu.edu/~dlopez/Simulations_\(published\).html](http://www4.ncsu.edu/~dlopez/Simulations_(published).html)

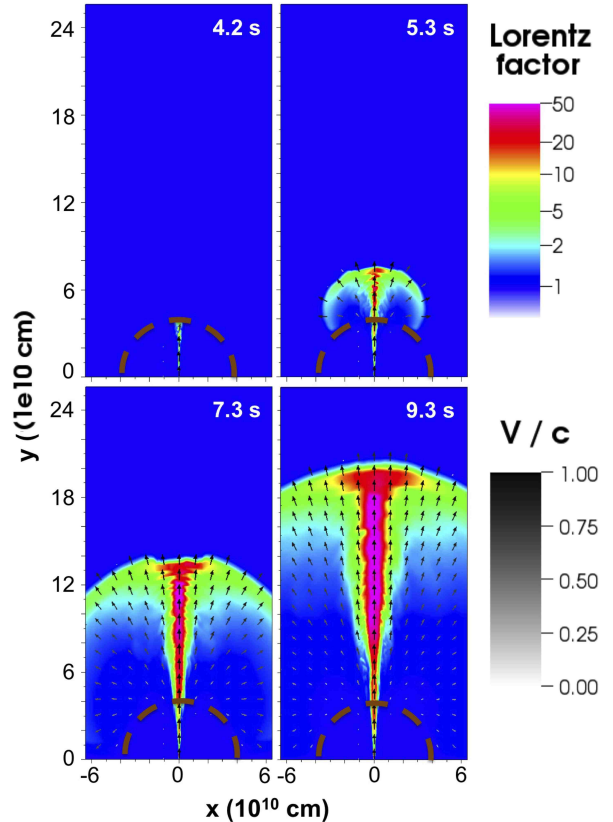


FIG. 5.— Lorentz factor stratification maps and velocity field for different timeframes (4.2 s; 5.3 s; 7.3 s; 9.3 s) for model 3D LR. The brown dashed line indicates the stellar surface. A movie of this figure is available in [http://www4.ncsu.edu/~dlopez/Simulations_\(published\).html](http://www4.ncsu.edu/~dlopez/Simulations_(published).html)

case has more turbulent-like structures. For both resolutions the low-density material (situated along the polar

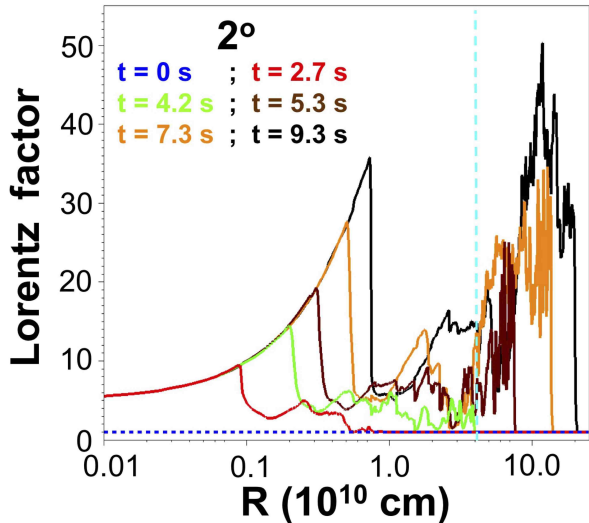


FIG. 6.— Same as Figure 4 but for the Lorentz factor. A movie of this figure is available in [http://www4.ncsu.edu/~dlopez/Simulations_\(published\).html](http://www4.ncsu.edu/~dlopez/Simulations_(published).html)

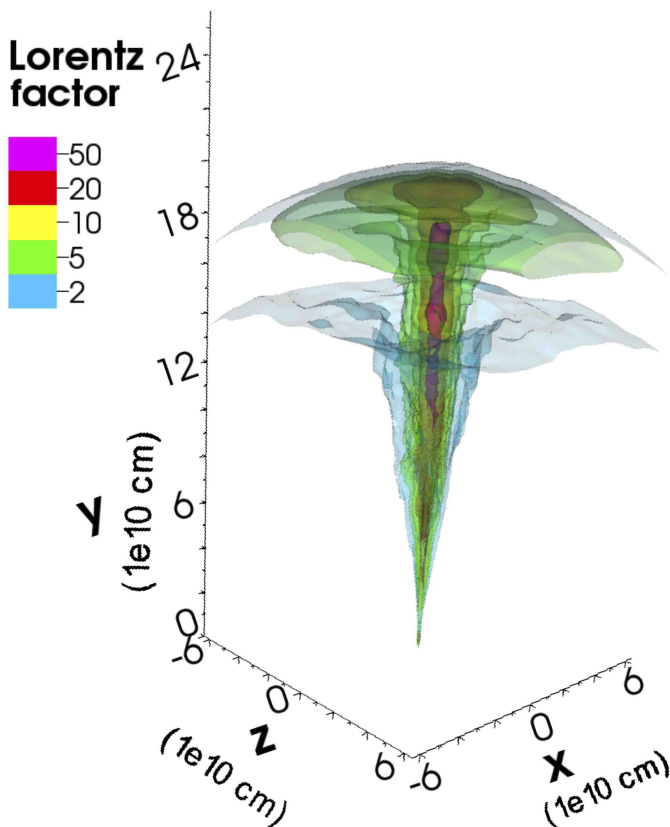


FIG. 7.— Lorentz factor isocontour map at $t=9.3$ s for model 3D LR. The isocontour levels correspond to: 2, 5, 10, 20 and 50. A movie of this figure is available in [http://www4.ncsu.edu/~dlopez/Simulations_\(published\).html](http://www4.ncsu.edu/~dlopez/Simulations_(published).html)

axis) has higher Lorentz factors compared to the material in the edge of the jet. The main difference, in qualitative terms, is that the high- Γ regions from the LR model are



FIG. 8.— Temporal evolution of the fraction of the volume that the two finest level occupied. The red line corresponds to the finest level ($\Delta \sim 10^7$ cm), and the blue and green lines to the second and third finest ($\Delta \sim 10^8$ cm).

split into smaller regions with lower Γ values in the HR model.

Another interesting aspect of our results is that the jet Lorentz factor morphology resembles the precessing jet case from Zhang et al. (2004). In our simulations though, the zig-zagging pattern in the Lorentz factor seems to be due to the ability of the high- Γ material to wobble around the star's rotation axis and propagate through paths of least resistance (see below for more details). The observation of this effect is likely facilitated by the fact that we have a larger dynamic range inside the star ($\delta_R = R_0/R_{\min} = 41$) compared to the one from Zhang et al. (2004) ($\delta_R = 8.8$). Thus, there is enough range inside the star for 3D instabilities to develop. In addition, the individual grid pixels in the Zhang et al. (2004) simulations was not square. Rectangular pixels generate more diffusion in the longest of the pixels direction, and results are therefore not as robust as those from square pixel grid simulations (where the diffusion is the same for all three directions).

Finally, we must remark that we do not claim to reach convergency. If we take the number of grid cells across the jet diameter as an estimate of the Reynolds number (Re) of the simulation, we see that at the present time we can only reach $Re \sim 200$. Such Reynolds number is approximately two orders of magnitude below the required Reynolds number in which the jet behavior is independent of the resolution (Birch & Eggers 1972). Unfortunately, numerical simulations as those presented in this study, with resolutions of at least two orders of magnitude finer are not feasible (due to technical difficulties) to date.

3.5. 2D vs 3D simulations

Finally, we checked how the evolution of the jet through the stellar envelope varies in two and three dimensional simulations. For this we ran an extra 2D numerical model with the same resolution ($\Delta = 1.25 \times 10^8$ cm), and the same parameter values (luminosity, R_i , θ_0 , Γ_0 , and η_0 , see section 2.2 for more

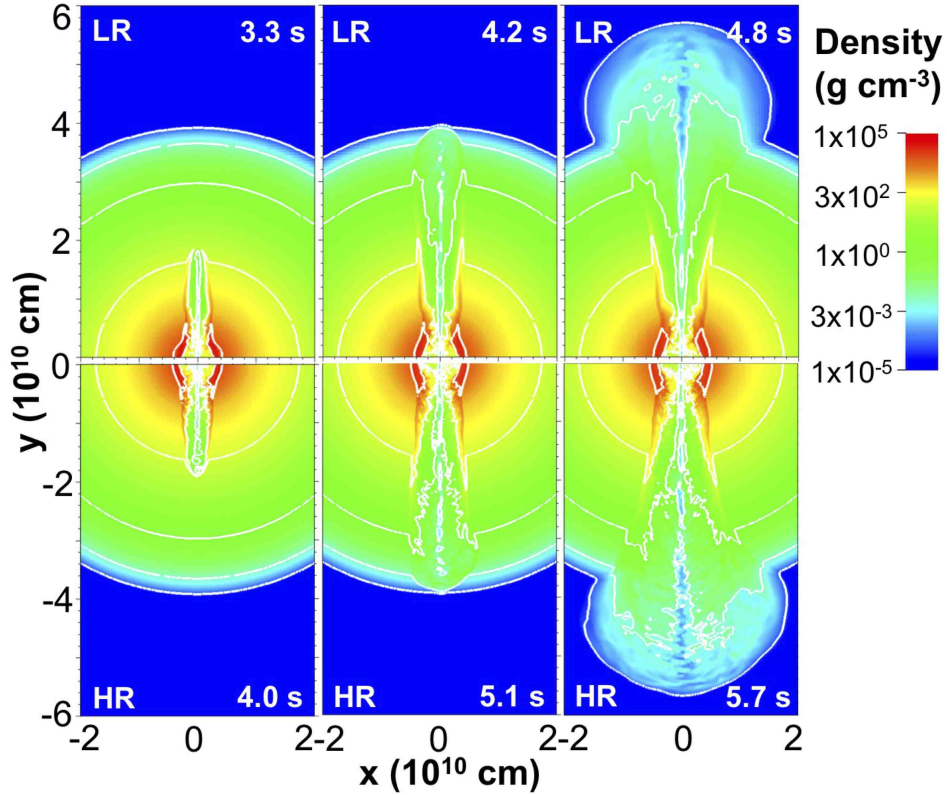


FIG. 9.— Density stratification maps (g cm^{-3}) for the 3D LR model (upper panels) and the 3D HR model (lower panels). For both models, we show representative timeframes from each of the two main phases (see text for discussion). The isocontour levels are the same as the ones indicated in Figure 1.

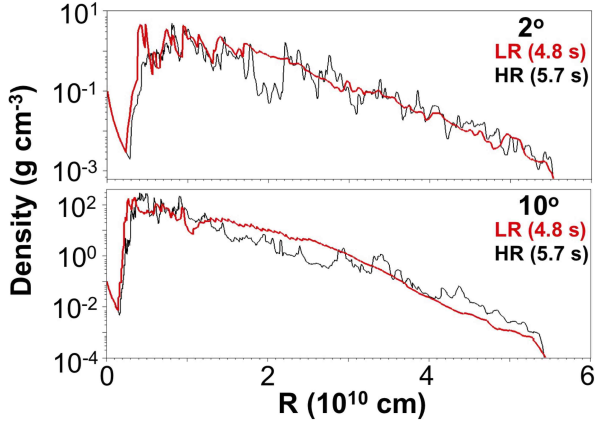


FIG. 10.— Radial density profile (g cm^{-3}) for the 3D LR model (red line) and the 3D HR model (black line). For both resolutions the 2° radial paths from the (+X,+Z) are shown in the upper panel, meanwhile the 10° paths are shown in the lower panel.

details) as the 3D HR case. Apart from the dimension difference from the 3D models, we assumed polar axis symmetry in the 2D simulation; thus in reality we only simulated half of the x-axis domain (i.e. $x_{\min}=0$).

The 2D simulation was carried out in cylindrical coordinates, with the polar axis coincident with the jet axis. In Figure 12 we show the density stratification maps for the 2D model at the two phases (as well as for the breakout time): a. $t < t_{\text{bo}}$; b. $t \approx t_{\text{bo}}$, and c. $t > t_{\text{bo}}$. The timeframes for each of the 2D phases shown in Figure 12 were

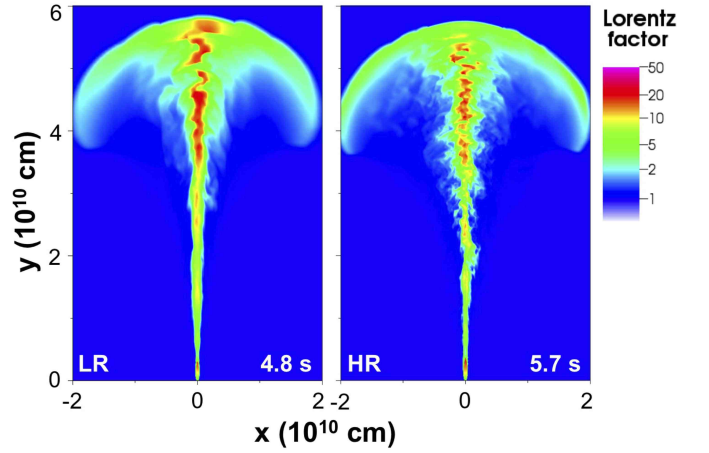


FIG. 11.— Lorentz factor stratification maps for the 3D LR (left panel), and the 3D HR model (right panel). For both resolution models, we show a representative timeframe for when the jet has already broken out of the star and is moving across the ISM.

chosen so that they resemble the correspondent timeframes from the 3D HR case. The basic morphology in the 2D case resembles that from the 3D model. In both cases we see a collimated jet that manages to drill through the stellar envelope. Apart from the polar axis symmetry imposed in the 2D model, there are many subtle differences between the 2D and 3D results:

1. The jet moves slower in the 2D model than in the

3D one (congruent with Zhang et al. (2004)). Thus, the 2D breakout time is larger ($t_{\text{bo}}^{2D}=7$ s) than for its correspondent 3D HR model. The reason for the slower jet's motion in the 2D model is the imposed symmetry. Not only is the jet axis-symmetric, but also the stellar material in front of the jet has to remain symmetric at all times. The SJ material can only escape from the jets plug sideways, so a lot of energy ends up going into accelerating this stellar material. In 3D models, instead, the jet can deflect slightly and go around the plug (rather than continuing to accelerate it, see below). Finally, the 2D jet model has a SJ material mildly broader ($\approx 20\%$) than its respective from the 3D model.

2. Even though the 2D model has the same resolution, the 2D jet presents less turbulent-like morphology than what is present in the 3D HR case. Also, the cocoon is less turbulent and broader in the 2D scenario, as is the case in the numerical study of Zhang et al. (2004).

3. Two low-density plumes are present in the 2D simulations (see right panel from Figure 12). It must be noted that due to the imposed axis-symmetry, the plumes actually correspond to a low-density torus around the jet head (if it were a three dimensional domain and not two dimensional). Such low-density torus is not present in any of the 3D simulations. This is somewhat similar to the findings from Zhang et al. (2004) where the head of the jet is noticeably different depending on the simulation dimensionality (either 2D or 3D).

4. As shown in the upper panel of Figure 14, where we plot the density profile along the polar axis for the 2D and 3D models, the 2D density radial profile is less turbulent and the depressions are more profound than those in the 3D density radial profile. Also, the SJ material is more dense by nearly two orders of magnitude in the 2D scenario close to the jet head.

In Figure 13 we show the Lorentz factor structure for the 2D case (once the jet has just broken out of the stellar surface). Even though the mushroom Γ structure forms, the 2D Lorentz factor morphology is noticeably different to that from the 3D HR case. The 2D Γ structure presents much less variability.

The 2D low-density regions have high Γ values of up to 15-20, values which are in agreement with those obtained by other 2D GRB jet studies (Zhang et al. 2004; Nagakura et al. 2011). The 2D model also has a SJ which is broader than that from the 3D case. As was the case for the density map in the 2D model, the head front of the cocoon has less turbulent-like Γ structures. In order to clarify this point, we show the radial Lorentz factor profile (along the polar axis) in Figure 14 (lower panel). Not only is a smoother radial profile present in the 2D, but also the high-density low- Γ relationship is present. The SJ from the 2D case is approximately two orders of magnitude more dense than from the 3D model, but has a rather smaller Γ value (of at most 5).

In order to analyze how much the jet changes direction as it drills through the progenitor star (and later through the ISM once the jet has broken out of the star) in a three dimensional domain, we plot in Figure 15 the energy density (U) map in the XZ plane. The XZ planes shown for each timeframe correspond to the position where the U centroid of the forward shock front was located at (see caption of Figure 15 for more details). Panels a through

d show the U map for when the jet is drilling through the stellar progenitor. In these it is noticeable how the centroid of the forward shock (CFS) does not have a gaussian like profile (it may have turbulent like behavior or even multiple spikes) and how the CFS wobbles around the polar axis finding the spot of least resistance to proceed. For example, notice how just before the jet breaks out of the star (panel d), the CFS is located far from the polar axis ($x=-0.3\times 10^{10}$ cm, $z=-0.6\times 10^{10}$ cm). Panel e shows how once the jet has broken out of the star and the cocoon has expanded thoroughly around the progenitor star, its correspondent CFS also expands and also remains far from the polar axis.

To further understand the deflection of the jet inside the pre-SN progenitor, we show the temporal evolution of the angle between the CFS and the polar axis (θ , black line in Figure 16). For a jet that is well aligned with the polar axis then the CFS displacement angle would yield $\theta = 0$, clearly in Figure 16 this is not the case and the jet wobbles inside the star (with θ oscillating between 0.1° and 2°). Hence, the jet moves faster in 3D than in 2D because it is able to wobble and move along the path with least resistance (apart from having a narrower jet-cocoon). Note that θ is always within the relativistic collimation angle ($1/\theta$, red line in Figure 16), thus the relativistic jet is causally connected at all times.

3.6. Limitations and comparison to other work

As with all numerical work, the choices made in carrying out the simulations reflect intentions and biases, and the current investigation lacks in several aspects. For example, similar to Zhang et al. (2004), Morsony et al. (2007, 2010), and Lazzati et al. (2009) we assumed that the star was static at all times which is clearly not the real case as the pre-SN for long GRBs have very high angular momentum values ($J>10^{15}$ cm² s) (Woosley & Heger 2006). We justify this by pointing out that the dynamical timescale of the pre-SN is of order close to hours. Then, since the integration time in our numerical simulations was of order 10 s, we were safe to assume that the pre-SN progenitor remained practically static at all times. In a previous study with a similar setup (Lazzati et al. 2011b) found that after 10^2 s the pre-SN stellar envelope had only expanded 2% of its original size.

Another issue which can be improved is the ISM distribution. The pre-SN progenitor that we use as the initial setup has no hydrogen shell since during its stellar evolution it was lost by the presence of a stellar wind (which will also affect the ISM surrounding the pre-SN star). So, in order to have full consistency the ISM should have a density profile which was affected by the pre-SN wind, i.e. a profile that follows a $\propto R^{-2}$ distribution (Zhang et al. 2003, 2004; Cannizzo et al. 2004; Nagakura et al. 2011). But since the jet-cocoon system is an ultra-relativistic flow, the density profile of the ISM will barely affect the jet once this has just broken out of the stellar surface (Morsony et al. 2007). In fact, the GRB-jet needs to reach $\sim 10^{14}$ cm for the ISM's profile to play a key role in the flow (Blandford & McKee 1976; De Colle et al. 2012). Thus, we were secure to assume that the ISM density was constant.

We use an adiabatic ($\gamma=4/3$) as our equation EOS (Zhang et al. 2003, 2004; Mizuta et al. 2006; Morsony

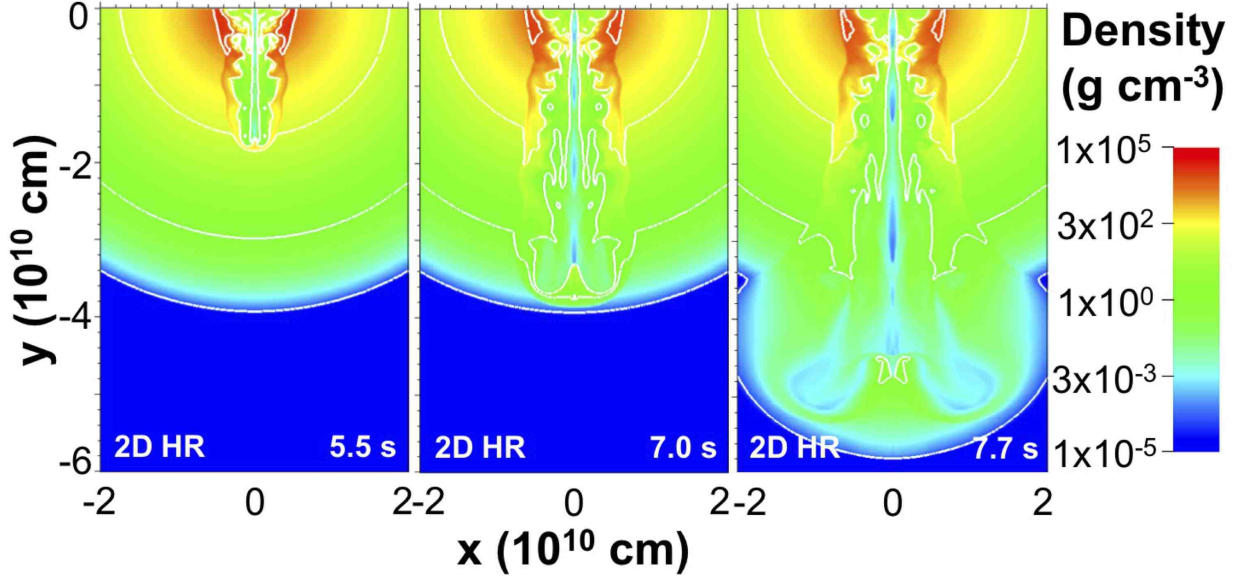


FIG. 12.— Density stratification maps (g cm^{-3}) for the 2D model. For this we show representative timesteps from each of the two main phases (see text for discussion). The isocontour levels are the same as the ones indicated in Figure 1.

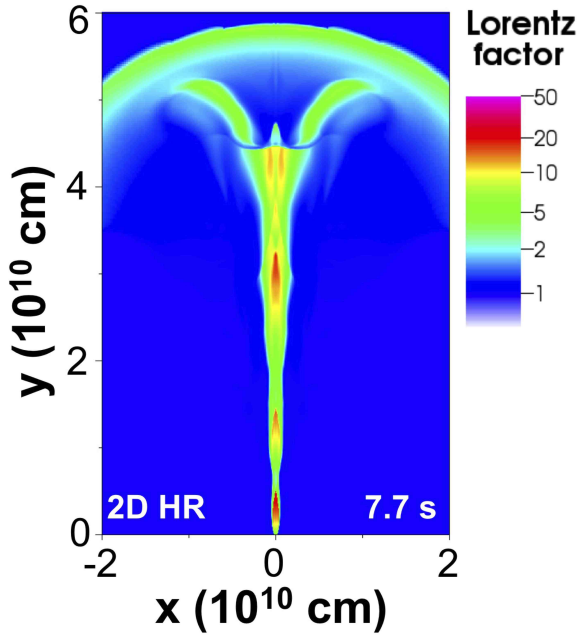


FIG. 13.— Lorentz factor stratification map for the 2D model at $t=7.7$ s.

et al. 2007, 2010; Lazzati et al. 2009; Nagakura et al. 2011). We do not take into account the neutrino pressure, nor do we take into account the gravitational effects from the central compact object. Even though it has been shown that close to the pre-SN's progenitor nucleus the neutrinos play an important role (López-Cámara et al. 2009), since the inner boundary was set so far away, $R_i \sim 10^9 \text{cm}$, equivalent to approximately 10^4 gravitational radii, from the region where neutrinos dominate (and where the compact object relativistic effects must be taken into consideration), the neutrino and relativistic effects were safely ignored.

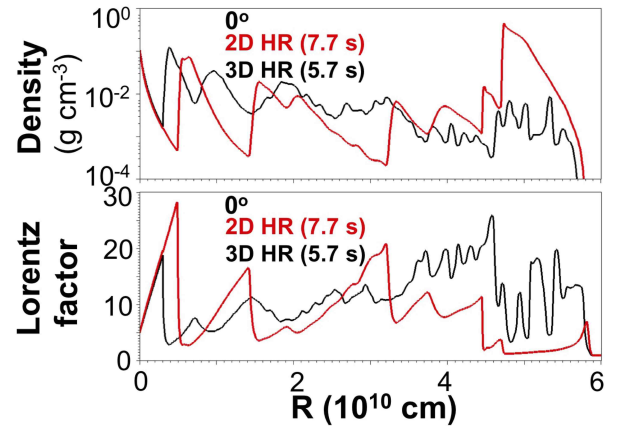


FIG. 14.— Radial density profile (g cm^{-3}) (upper panel), and the radial Lorentz factor (bottom panel) for both the 2D model (red line) and the 3D model (black line) for the timeframe when the jet has broken out of the star. For both models the path is a polar axis (0°) radial paths from the $(+X,+Z)$ quadrant.

Since the follow up of newly formed elements was not the aim of this study and that the calculation of such new elements would have not permitted us to study the flow both at an adequate resolutions and for the long times desired, nuclear burning was not included. Also, even though magnetic fields will affect the emissivity of the jet (Mizuta et al. 2006), and could even give origin to variability in the light curve (Balbus & Hawley 1998), they were disregarded due to the technical difficulties when following a magnetized relativistic flow with an adaptive mesh code.

4. CONCLUSIONS

We present, for the first time, 3D AMR simulations of GRB jets expanding inside a realistic pre-SN progenitor and then flowing through the interstellar medium. Our numerical simulations, confirm that relativistic jets

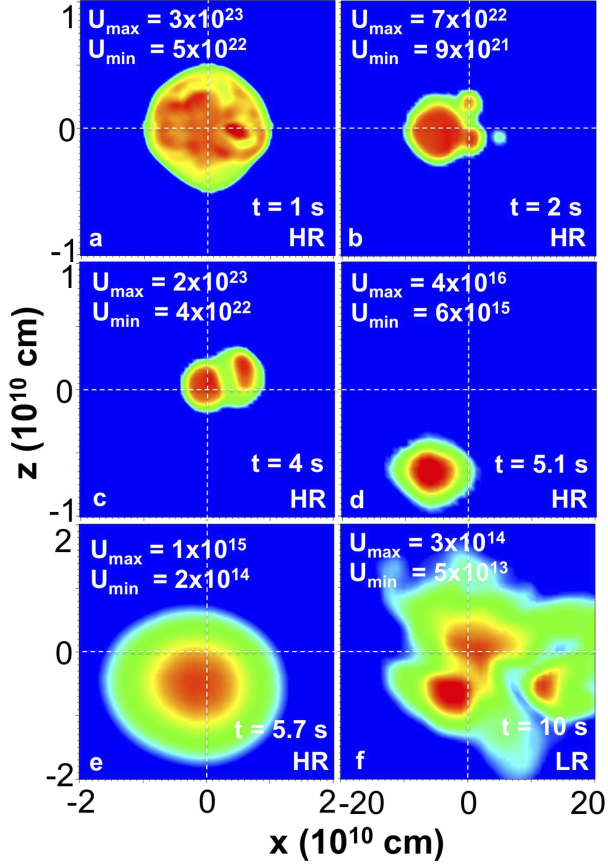


FIG. 15.— Energy density (erg cm^3) XZ stratification maps for the centroid of the head front of the jet-cocoon structure for different times. Panels a through e correspond to the 3D HR model, panel f correspond to the 3D LR model. Panel a. $t=1\text{s}$, b. $t=2\text{s}$, c. $t=4\text{s}$, d. $t=5.1\text{s}$, e. $t=5.7\text{s}$, f. $t=10\text{s}$; have the XY plane located at $Y/(10^{10}\text{ cm})=1.3, 3.3, 18.9, 39.9, 57.1$ (respectively). In each panel the maximum and minimum values of the forward shock’s energy density centroid (in erg cm^3) is indicated. Notice how some panels have different scales.

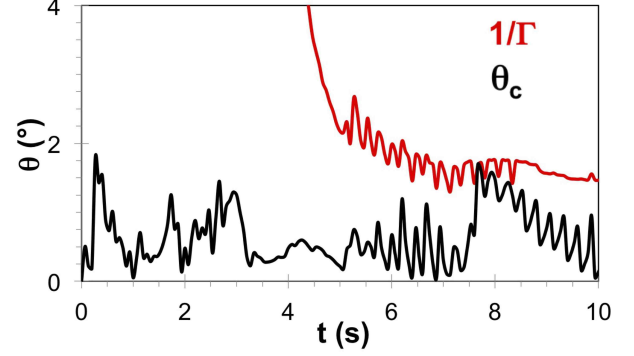


FIG. 16.— Temporal evolution of the CFS (black line), and the relativistic collimation angle (red line).

can propagate and break out of the progenitor star while remaining relativistic.

The morphology is divided into two main phases:

1. Pre- t_{bo} . During this phase the jet head moves at mildly relativistic velocities ($\sim c/2$) inside the progenitor’s stellar envelope.
2. Post- t_{bo} . Once the jet breaks out of the surface, it accelerates and reaches Lorentz factors of order $\Gamma \sim 50$.

The initial progenitor density profile is reshaped by the forward and reverse shocks. The material between the forward and reverse shocks break the two-dimensional symmetry in the numerical simulations.

We obtain similar behavior independently of the numerical resolution. The resolution does not affect in great detail the flow and the morphology in each phase is well reproduced. Still, the amount of turbulence and variability observed in the simulations is higher for higher resolutions. Also, for finer numerical resolutions the jet moves slower; and regions with high Lorentz factors break up into smaller regions with lower Γ values.

The propagation of the jet head inside the progenitor star is slightly faster in 3D simulations compared to 2D ones at the same resolution. This behavior is due to the fact that the jet in 3D simulations is narrower and can wobble around the jet axis finding the spot of least resistance to proceed. Most of the jet properties, such as density, pressure, and Lorentz factor, are only marginally affected by the dimensionality of the simulations and therefore results from 2D simulations can be considered reliable. If, instead, more detailed properties such as variability are to be investigated, simulations carried out in the proper dimensionality (i.e. 3D) are required.

We thank S.E. Woosley and A. Heger for making their pre-SN models available, and the referee for comments, suggestions and constructive criticism which helped improve the original version of the manuscript. The software used in this work was in part developed by the DOE-supported ASC/Alliance Center for Astrophysical Thermonuclear Flashes at the University of Chicago. This work was supported in part by the Fermi GI program grants NNX10AP55G and NNX12AO74G (D.L. and D.L.-C.). B.J.M. is supported by an NSF Astronomy and Astrophysics Postdoctoral Fellowship under award AST-1102796.

REFERENCES

- Aloy, M. A., Ibáñez, J. M., Miralles, J. A., & Urpin, V. 2002, *A&A*, 396, 693
- Aloy, M. A., Müller, E., Ibáñez, J. M., Martí, J. M., & MacFadyen, A. 2000, *ApJ*, 531, L119
- Balbus, S. A. & Hawley, J. F. 1998 *Rev. Mod. Phys.*, 70., 1
- Birch, S. F., & Eggers, J. M. 1972, In: *Free Turbulent Shear Flows*, Conf. Proc. NASA-SP-321, Vol. I, 11-40
- Blandford, R. D., & McKee, C. F. 1976, *Physics of Fluids*, 19, 1130
- Bromberg, O., Nakar, E., Piran, T., & Sari, R. 2011, *ApJ*, 740, 100
- Cannizzo, J. K., Gehrels, N., & Vishniac, E. T. 2004, *ApJ*, 601, 380
- De Colle, F., Ramirez-Ruiz, E., Granot, J., & Lopez-Camara, D. 2012, *ApJ*, 751, 57
- Fryxell, B., Olson, K., Ricker, P., et al. 2000, *ApJS*, 131, 273
- Gómez, E. A., & Hardee, P. E. 2004, *Gamma-Ray Bursts: 30 Years of Discovery*, 727, 278
- Hjorth, J., Sollerman, J., Møller, P., et al. 2003, *Nature*, 423, 847
- Khokhlov, A. M., Höflich, P. A., Oran, E. S., et al. 1999, *ApJ*, 524, L107
- Lazzati, D., & Begelman, M. C. 2005, *ApJ*, 629, 903
- Lazzati, D., Blackwell, C. H., Morsony, B. J., & Begelman, M. C. 2011a, *MNRAS*, 411, L16
- Lazzati, D., Morsony, B. J., & Begelman, M. C. 2009, *ApJ*, 700, L47
- Lazzati, D., Morsony, B. J., & Begelman, M. C. 2010, *ApJ*, 717, 239
- Lazzati, D., Morsony, B. J., & Begelman, M. C. 2011b, *ApJ*, 732, 34
- Lazzati, D., Morsony, B. J., Blackwell, C. H., & Begelman, M. C. 2012, *ApJ*, 750, 68
- Lindner, C. C., Milosavljević, M., Couch, S. M., & Kumar, P. 2010, *ApJ*, 713, 800
- Lindner, C. C., Milosavljević, M., Shen, R., & Kumar, P. 2012, *ApJ*, 750, 163
- López-Cámara, D., Lee, W. H., & Ramirez-Ruiz, E. 2009, *ApJ*, 692, 804
- López-Cámara, D., Lee, W. H., & Ramirez-Ruiz, E. 2010, *ApJ*, 716, 1308
- MacFadyen, A. I., & Woosley, S. E. 1999, *ApJ*, 524, 262
- MacFadyen, A. I., Woosley, S. E., & Heger, A. 2001, *ApJ*, 550, 410
- Maeda, K., & Nomoto, K. 2003, *ApJ*, 598, 1163
- Matzner, C. D. 2003, *MNRAS*, 345, 575
- Mizuta, A., & Aloy, M. A. 2009, *ApJ*, 699, 1261
- Mizuta, A., Yamasaki, T., Nagataki, S., & Mineshige, S. 2006, *ApJ*, 651, 960
- Morsony, B. J., Lazzati, D., & Begelman, M. C. 2007, *ApJ*, 665, 569
- Morsony, B. J., Lazzati, D., & Begelman, M. C. 2010, *ApJ*, 723, 267
- Nagakura, H., Ito, H., Kiuchi, K., & Yamada, S. 2011, *ApJ*, 731, 80
- Ramirez-Ruiz, E., Celotti, A., & Rees, M. J. 2002, *MNRAS*, 337, 1349
- Sari, R., Piran, T., & Halpern, J. P. 1999, *ApJ*, 519, L17
- Stanek, K. Z., Matheson, T., Garnavich, P. M., et al. 2003, *ApJ*, 591, L17
- Wang, P., Abel, T., & Zhang, W. 2008, *ApJS*, 176, 467
- Wheeler, J. C., Meier, D. L., & Wilson, J. R. 2002, *ApJ*, 568, 807
- Woosley, S. E. 1993, *ApJ*, 405, 273
- Woosley, S. E., Bloom, J. S. 2006, *ARA&A*, 44, 507
- Woosley, S. E., & Heger, A. 2006, *ApJ*, 637, 914
- Zhang, W., Woosley, S. E., & Heger, A. 2004, *ApJ*, 608, 365
- Zhang, W., Woosley, S. E., & MacFadyen, A. I. 2003, *ApJ*, 586, 356